JOURNAL OF PROPULSION AND POWER
Vol. 20, No. 5, September–October 2004

Rotor-Generated Vane Row Off-Design Unsteady Aerodynamics Including Dynamic Stall, Part 2

Roy D. Fulayter,* Patrick B. Lawless,† and Sanford Fleeter‡
Purdue University, West Lafayette, Indiana

Blade row interaction effects on airfoil unsteady aerodynamics are investigated, particularly at off-design operating conditions. The specific problem addressed is off-design unsteady aerodynamics including dynamic stall due to the interaction of rotor-generated wakes with a downstream vane row. This is accomplished by obtaining detailed three-dimensional rotor–stator unsteady aerodynamic blade row interaction data in a low-speed axial-flow research compressor. These detailed data include measurements of the rotor wake generated unsteady aerodynamic forcing function to the downstream stator, the resultant stator vane steady and unsteady aerodynamic response, and particle image velocimetry (PIV) measurements of the time-variant stator midspan vane-to-vane flowfield. The rotor wake-generated forcing function and downstream stator steady and unsteady aerodynamic response data are described, with the time-variant PIV flowfield data described in the companion paper.

Nomenclature

C = chord
C_p = unsteady pressure coefficient
p_0 = freestream pressure
p^* = unsteady nondimensional pressure
U = mean axial velocity
v_m^* = transverse dimensionless perturbation velocity

Introduction

DYNAMIC stall, an unsteady flow phenomenon, refers to unsteady flow separation with the airfoil transitioning in and out of the stalled condition. For an airfoil oscillating in torsion, dynamic stall typically begins at an angle of attack greater than the static stall angle, that is, the flow dynamics delay the onset of stall. Thus, an oscillating airfoil can exceed the steady stall angle without flow separation, which results in additional unsteady lift.

This additional unsteady lift is associated with a vortex that forms on the airfoil during the pitching motion. For an airfoil at moderate angle of attack, the flow around the airfoil is essentially inviscid. As the angle of attack increases, signs of boundary-layer separation begin at the trailing edge and move toward the leading edge. A vortex forms near the leading edge, grows, and convects downstream along the airfoil. This is accompanied by a significant lift overshoot, followed by flow separation, an increase in pitching moment, and a subsequent flow reattachment starting at the leading edge.[1] This behavior takes the form of a limit cycle (Figure 1), with the time-mean angle of attack and lift at stall sometimes exceeding that experienced in steady flow.

A number of studies have focused on dynamic stall in isolated airfoils, including Carr and McCroskey,[2] Zaman et al.,[3] and Gendrich et al.[4] Such studies are motivated by applications such as helicopter rotors, where cyclic changes in incidence can trigger the event. Dynamic stall effects can also occur in turbomachinery blading, although few studies have investigated this issue. Ehrlich and Fleeter[5] reported dynamic stall effects in a cascade with simple flat plate geometry that was oscillating in chordwise bending. Henderson and Fleeter[6] also observed indirect evidence for a wake-induced negative incidence dynamic stall condition in a low-speed compressor stage. Unfortunately, both of these studies were primarily focused on other issues in unsteady aerodynamics and did not pursue an investigation of the dynamic stall phenomenon itself.

When a multistage compressor is operating at part-speed conditions, the front stages are typically at high positive mean incidence while the rear stages are at low negative mean incidence. Thus, the front stages can exhibit periodic positive-incidence separation while the rear stages can be induced to a periodic negative-incidence separation under the effect of wake impingement. Dynamic stall phenomena occurring in rotating turbomachinery blade rows are quite different from those encountered on an oscillating isolated airfoil. For example, consider an isolated airfoil at low angle of attack (unstalled) oscillating in torsion (Figure 2).

The effect of reduced frequency on the unsteady moment as a function of the instantaneous angle of attack is a loop predominantly due to a Theodorsen-type phase lag, conferring instability (energy into the airfoil). The dominating aerodynamic mechanism for producing this loop is a classical attached flow aerodynamic phase lag.

If the airfoil is now set at an angle of attack near or somewhat exceeding the steady stall limit, the loops may demonstrate a quite different behavior for an identical assumed airfoil motion (Figure 3) because they are now dominated by the dynamic stall mechanism.

Dynamic stall is now playing a predominant role in the unsteady moment loop and may even shift the sense of loop traversal to produce an instability from an otherwise stable situation. The effect of dynamic stall on stability can, thus, be dramatic.

Dynamic stall events, namely, flow separation, formation of the vortex, movement of the vortex, and reattachment, take a finite time to develop. However, once the flow is separated, the dynamic stall event introduces two important physical consequences. The first is the hysteresis produced by the lag and asymmetry of the unsteady aerodynamic forces with respect to the airfoil motion. During dynamic stall, isolated airfoils exhibit large hysteresis loops in both lift and torsion moment as a function of the airfoil angle of attack θ. Hence an airfoil with positive pitch rate $\dot{\theta}$ stalls at an angle greater than the steady or static stall angle $\theta_{\text{st-stall}}$, termed stall delay, whereas the stall recovery during negative pitch rate $\dot{\theta}$ occurs at an angle of attack less than $\theta_{\text{st-stall}}$. This is in contrast to the steady or quasi-steady case where no hysteresis is produced because the flowfield adjusts immediately to each change in angle of attack. The second consequence of dynamic stall is aerodynamic damping. When the

Presented as Paper 2002-3542 at the AIAA Propulsion Conference, Indianapolis, IN, 2 July 2003; received 15 July 2003; revision received 15 December 2003; accepted for publication 15 December 2003.

*Research Assistant, School of Mechanical Engineering. Student Member AIAA.
†Associate Professor, School of Mechanical Engineering. Member AIAA.
‡McAllister Distinguished Professor, School of Mechanical Engineering. Fellow AIAA.

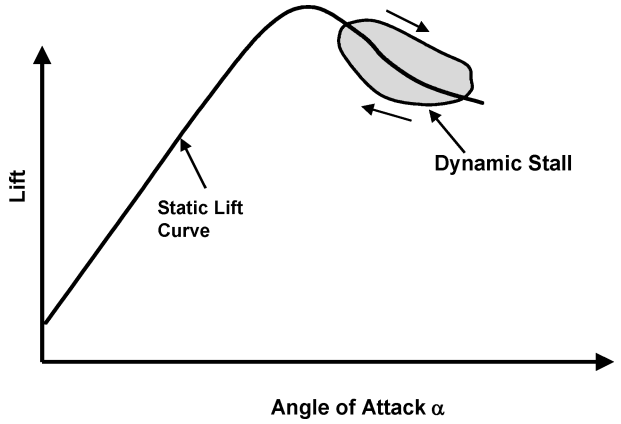

Fig. 1 Dynamic stall limit-cycle behavior.

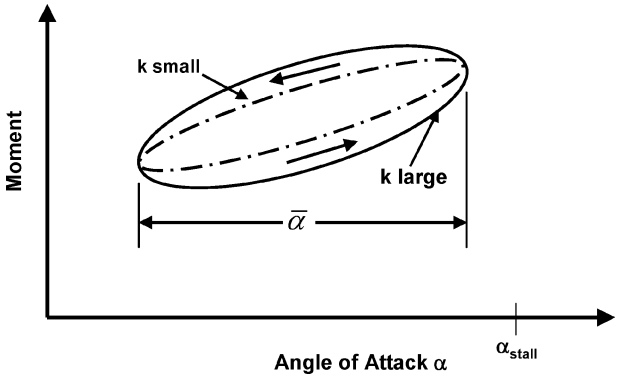

Fig. 2 Moment of unstalled airfoil in torsional motion.

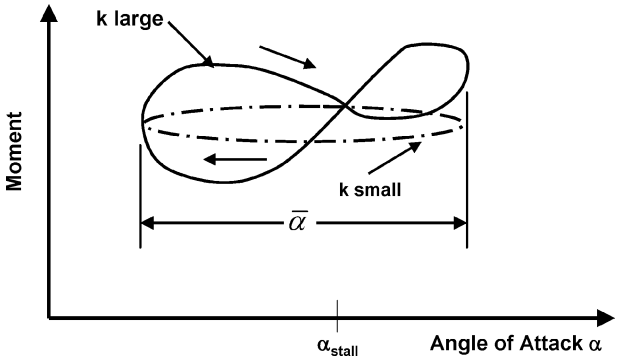

Fig. 3 Moment of airfoil with dynamic stall.

aerodynamic damping is negative, the airfoil extracts energy from the flow, which results in flutter. Stall flutter occurs when the airfoil oscillates into and out of stall. As the instantaneous angle of attack varies, the torsion moment exhibits loops corresponding to negative and positive aerodynamic damping.

This two-part paper is directed at characterizing multistage interaction effects on airfoil unsteady aerodynamics, particularly at off-design operating conditions. The specific problem addressed is off-design unsteady aerodynamics including dynamic stall due to the interaction of rotor-generated wakes with a downstream vane row. This is accomplished by obtaining detailed three-dimensional rotor–stator unsteady aerodynamic blade row interaction data in a low-speed axial-flow research compressor. These detailed data include measurements of the rotor wake generated unsteady aerodynamic forcing function to the downstream stator, the resultant stator vane steady and unsteady aerodynamic response, and particle image velocimetry (PIV) measurements of the time-variant stator midspan vane-to-vane flowfield. This portion of the paper describes the rotor wake generated forcing function and downstream stator steady and unsteady aerodynamic response data, with the time-variant PIV flowfield data described in part 1 (Key et al.[7]).

Research Facility

The Purdue Annular Cascade Research Facility (refer to Key et al.[7]) is an open-loop drawthrough wind tunnel with a maximum test section velocity of 220 ft/s (67.06 m/s). A honeycomb section and acoustically treated inlet plenum condition the flow before it is accelerated through a bellmouth and enters the test section. After the flow exits the test section, it enters a diffuser and then discharges into a large plenum. Downstream of the plenum, a centrifugal blower powered by a 300-hp (223.7-kW) induction motor draws the air through the test section. Damper vanes upstream of the blower adjust the flow rate through the facility. In the test section, a 50-hp (37.28-kW) dc motor powers an axial-flow rotor with the rotor speed controlled by a variable-speed drive. Because the primary energy source to the flow is the downstream blower, the axial velocity through the test section can be set independently from the rotor speed.

The rotor blades are attached to a T slot, machined into the hub of the rotor disk, via sliding cars to allow the spacing and number of blades to be varied. For this experiment, 19 rotor blades, at a stagger angle of −30 deg at midspan, are evenly spaced around the annulus with an angular displacement of 18.95 deg between blades. The rotor airfoil profile is a NACA 65A010 thickness distribution superimposed on a NACA $a = 1.0$ uniform load meanline. The blades have 8.2 deg of twist from hub-to-tip with a chord of 5.0 in. (12.7 cm) and span of 5.9 in. (14.99 cm).

The stator configuration has 18 vanes uniformly spaced with an angular displacement of 20 deg between vanes. The stator vanes are constructed with a NACA 65A012 thickness distribution on a 30 deg circular arc meanline. The chord and span are 6.0 in. (15.24 cm.), with the stator stagger angle varied to achieve different stator mean loading levels. The vanes have no twist.

Technical Approach

The rotor wake forcing function is characterized in isolation by removing the stators. The velocity is measured using a three-channel TSI Incorporated IFA-100 intelligent flow analyzer and a custom Auspex 3-sensor hotwire probe. The data are acquired at a location 20% downstream of the rotor trailing edge, at spanwise locations from 10 to 95%.

To characterize the steady and unsteady response, two stators are instrumented for the vane surface steady and unsteady surface pressure measurements. Static pressure taps are utilized for the vane surface steady pressure measurement with the uncertainty in the measured pressure being 0.06%. High-frequency response PCB Piezotronics, Inc. 103A dynamic pressure transducers are either flush mounted with the airfoil surface or mounted inside the airfoil and connected to the surface via a machined passage. The unsteady surface pressure transducers are calibrated to a reference transducer with an estimated uncertainty of 1% (Henderson[8]). The steady and unsteady airfoil surface pressures are measured at 12 chordwise locations between $x/C = 0.025$ and 0.95 on each surface, as shown in Fig. 4.

Because the vanes are two dimensional, spanwise repositioning of the instrumented airfoils was enabled by making them longer than the span of the cascade and allowing them to slide through the endwalls to achieve measurement capability at any spanwise location. Data from 50 to 95% were acquired. The axial spacing between the rotor and stators was 20% of the rotor chord.

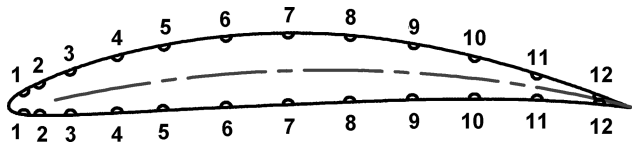

Fig. 4 Distribution of measurement locations along the stator.

The test cases of interest here, as described in Key et al.[7] are those of −22 and −17 deg of vane stagger. This corresponds to a mean flow angle of attack (AOA) of −10 and −5 deg, respectively. The rotor speed is 391 rpm, which corresponds to a reduced frequency of 3.1. The Reynolds number based on the stator chord is 3.8×10^5. In Key et al.[7] dynamic stall was seen to occur as an isolated event for the −5 deg AOA (−17 deg stagger) case and was seen to modulate a steady separation at −10 deg AOA (−22 deg stagger).

Results

Rotor Wake Forcing Function

The rotor exit flowfield data, that is, the aerodynamic forcing function to the downstream stator row, are acquired with the stator row removed. These data define the mean and unsteady axial, tangential, and radial velocity components that comprise the measured wake. The spanwise variation of the mean axial, tangential, and radial velocity components U, V, and W normalized by the magnitude of the mean flow axial velocity are shown in Fig. 5.

The mean axial velocity data show that the outer annulus wall boundary layer extends to approximately 85% span, and the inner annulus wall boundary layer extends to approximately 10% span. The uncertainty in all three components of the velocity is below 2% of the velocity magnitude.

The measured tangential and radial unsteady velocity perturbations are shown in Fig. 6 for 10–95% span for two rotor blade-pass periods. The data are ensemble averaged by the blade-pass period with two rotor passes reproduced from the ensembled data.

The perturbation velocity is defined as the unsteady portion of the local velocity signal. The flow is similar from 20 to 80% span with the 10 and 90% span locations similar in the wake. The largest radial velocity perturbations are seen at 95% span, with the smallest radial velocity perturbations at midspan. The unsteady tangential velocity is slightly larger than the unsteady radial velocity at all spanwise locations. In the rotor wake, the perturbation velocity vector turns radially toward the tip. The unsteady tangential velocity is positive in the rotor wake. A positive tangential velocity is in the direction of rotor rotation. The magnitude of the radial velocity perturbation increases with span with the 95% span data nearly double the magnitude at any other span.

The axial and tangential velocity perturbations are shown in Fig. 7 for 50, 90, and 95% span. Also shown in Fig. 7 are the mean velocity triangles. The data are ensemble averaged by the blade-passing period with two rotor passes reproduced from the ensembled data. The velocity vectors in the wake align with the mean relative velocity vector, and the velocity deficit in the wake decreases toward the tip.

A large velocity perturbation immediately follows the wake at 95% span, a possible artifact of the rotor tip clearance vortex. Chen et al.[9] showed that for axial flow compressors the trajectory of the vortex is based on the mean rotor loading and is independent of the tip clearance. Therefore, a measurement of the tip clearance is not needed to predict the location of a rotor tip vortex. The second disturbance in the velocity perturbations at 95% span is consistent with the location of a rotor tip clearance vortex from the Chen et al.[9] model.

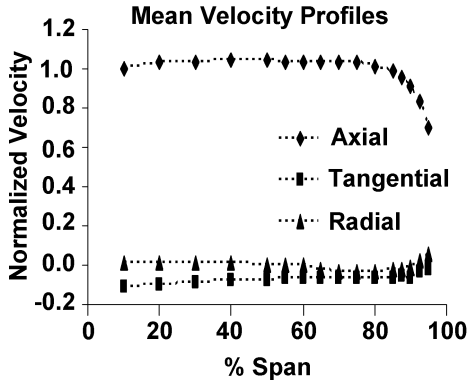

Fig. 5 Mean axial, tangential, and radial velocity components.

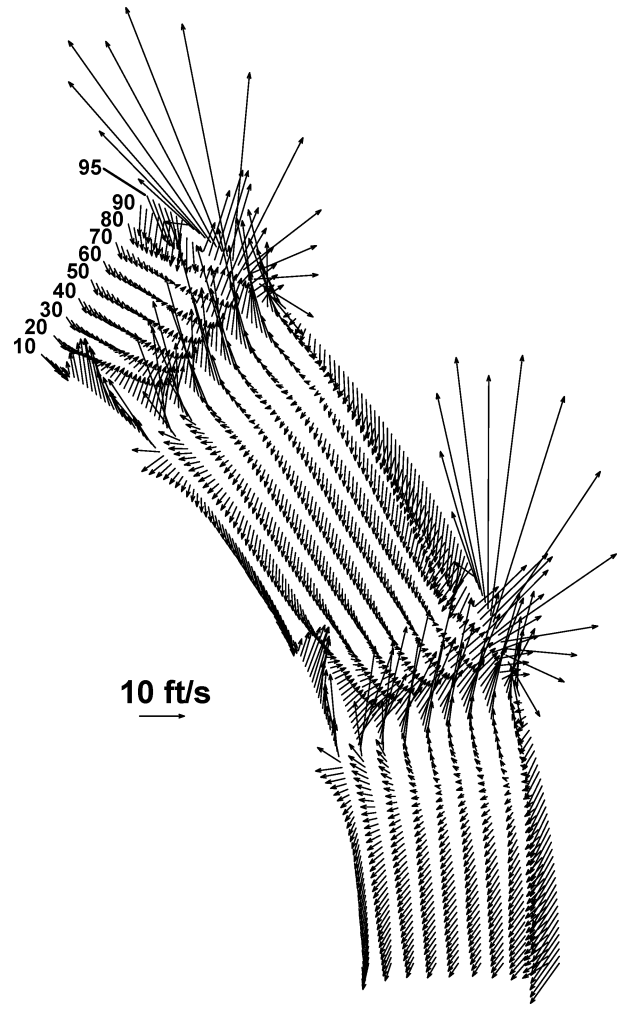

Fig. 6 Wake forcing function: tangential and radial velocity perturbations from 10 to 95% span.

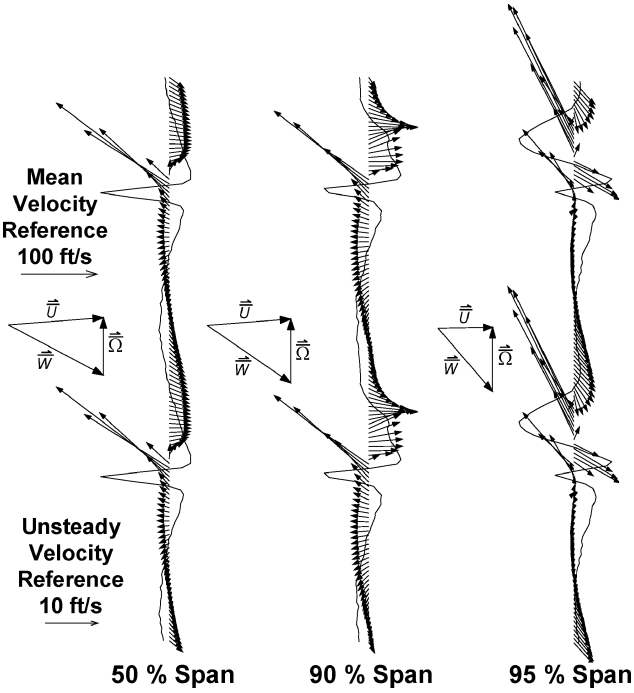

Fig. 7 Wake forcing function: tangential and axial velocity perturbations for 50, 90, and 95% span.

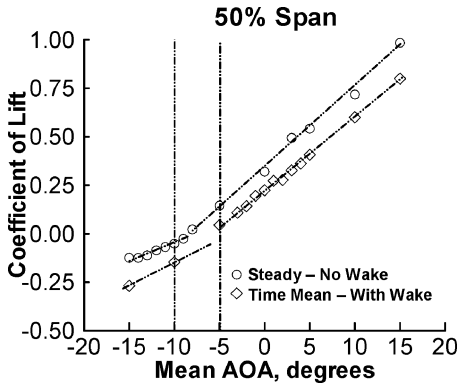

Fig. 8 Steady and time-mean stall points, 50% span.

In summary, the velocity perturbations are three dimensional, with the tip region shown to contain smaller perturbations in the wake and large perturbations due to a rotor tip vortex immediately following the wake compared to midspan.

Vane Mean Response

The vane row mean response is characterized by the mean pressure coefficient $\bar{C}_p(x)$ and the mean lift $\bar{L}$,

$$\bar{C}_p(x) = \frac{p(x) - P_0}{\frac{1}{2}\rho_0 U^2} \tag{1}$$

$$\bar{L} = \int_{0.025}^{0.95} \overline{C_{\Delta p}(x^*)}\, \mathrm{d}x^* \tag{2}$$

where $p(x)$ is the surface mean pressure, p_0 is the midspan freestream static pressure, the density ρ_0 and the mean flow velocity U are midspan values, $x^* = x/C$ is the nondimensional distance along the chord, and the lift is calculated utilizing the trapezoidal rule. The effect of unsteady flow on the mean response of the vane row is determined by measuring the mean lift in a steady flow, that is with the rotor blades removed, and in the unsteady flow generated by the rotor.

Steady and time-mean lift coefficients for 50% span as a function of mean AOA are presented in Fig. 8. The steady (no-wake) negative incidence stall point is located near −10-deg AOA, where the slope of the lift coefficient decreases as the mean AOA decreases. In the unstalled region, the slope of the lift curve is nearly constant with AOA. For the case with the rotor in place, the time-mean lift is shown to continue past the −10 deg steady stall point with more positive slope than the earlier case, as expected for dynamic stall.

Vane Unsteady Response

Unsteady Pressures at Midspan

The unsteady vane response to the wake forcing function is characterized by the surface pressures measured along the vane chord at 50% span. Figures 9, 10, and 11 present the unsteady pressure scaled with dynamic pressure for the cases of −12, −17, and −22 deg stagger, respectively. These cases correspond to 0, −5, and −10 deg mean AOA, with the latter two cases being the subject of the PIV study presented in Key et al.[7] The 0 deg mean AOA case is presented for comparison purposes because dynamic stall was not indicated by the mean flow results of Fig. 8. The pressures along the suction and pressure sides of the vane are given as fraction of chord for 10 positions of the rotor relative to the vane (RRP) over a blade-pass cycle. At 0 deg mean AOA, (Fig. 9), the blade response seems relatively benign, with most of the activity associated with the wake forcing function located near the leading edge. However, Fig. 10 shows that, at −5 deg AOA, an unsteady pressure disturbance is seen to propagate down the pressure surface of the vane beginning at 0% RRP. As the disturbance moves down the vane, the magnitude of the unsteady pressure decreases.

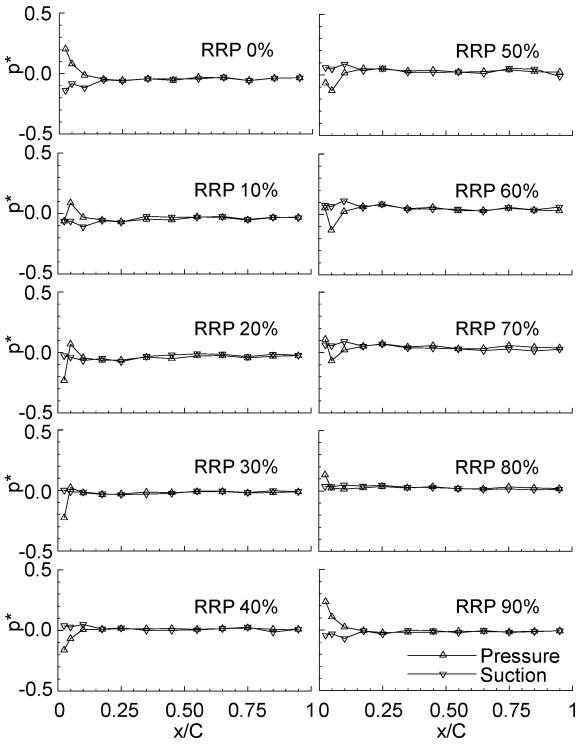

Fig. 9 Vane surface unsteady pressure over a blade pass cycle: 50% span, and 0-deg AOA (−12 deg stagger).

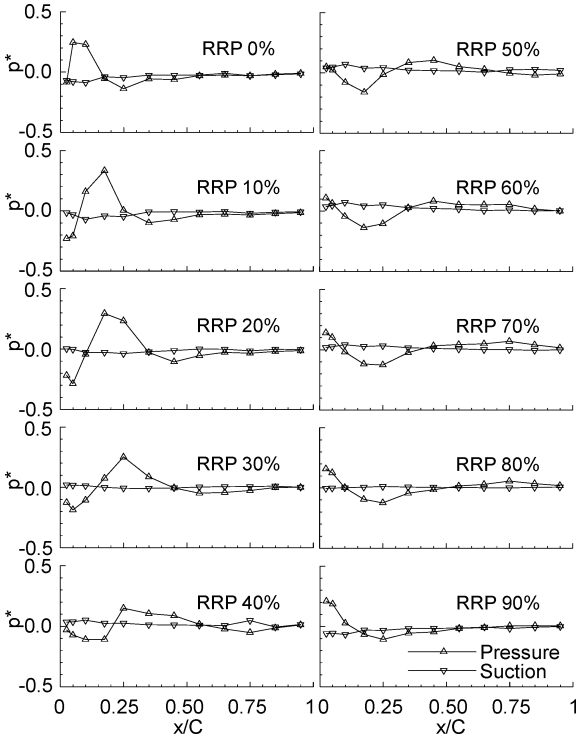

Fig. 10 Vane surface unsteady pressure over a blade pass cycle: 50% span and −5 deg AOA (−17 deg stagger).

This response correlates well with the PIV data presented in Key et al.,[7] where a transient separation bubble at the leading edge was seen to collapse and generate a vortex that moved down the vane surface. The vorticity data at 40% RRP shows the vortex located at approximately 25% chord, which agrees well with location of the disturbance in the unsteady pressure data. By 70% RRP, the vortex was shown to leave the vane surface. The disturbance in the unsteady pressure decreased at 50 and 60% RRP and was negligible at 70% RRP.

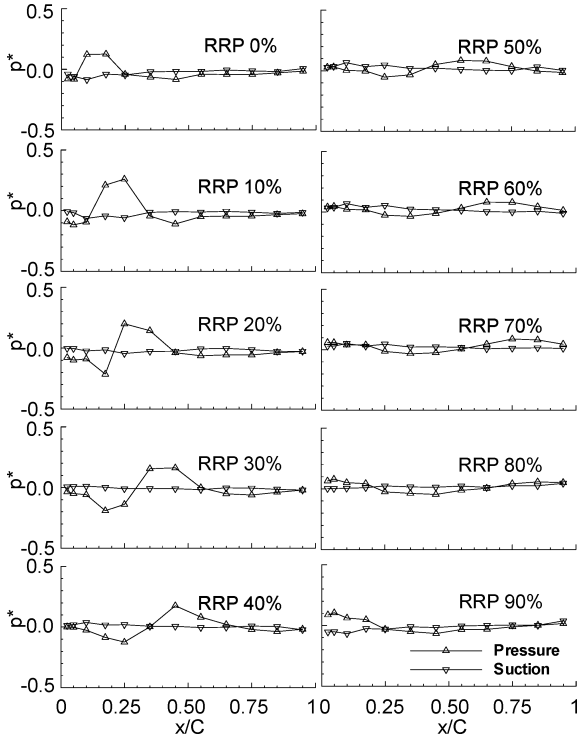

Fig. 11 Vane surface unsteady pressure over a blade-pass cycle: 50% span and −10 deg AOA (−22 deg stagger).

In Fig. 11, the case of −10 deg mean AOA is shown. As identified in Key et al.,[7] in this case, there is an ever-present separation bubble located on the pressure side leading edge, which is modulated in extent by the wake passage event. In Fig. 11, we see the net effect on unsteady vane response is similar to the preceding case, albeit with a reduction in the initial leading-edge unsteady pressure peak.

In summary, it is apparent that the dynamic stall process observed here for a compressor stage is an inherently different process than the isolated airfoil dynamic stall. As seen in the vorticity field plots of the companion paper (Key et al.[7]), no trailing edge vorticity, which is indicative of a trailing edge vortex, is seen as described by Visbal[10] with the constant pitch airfoil. Rather, it appears that the dynamic stall is triggered solely by the wake passing the leading edge of the airfoil. This wake triggered dynamic stall is a result of the wake decreasing the magnitude of the AOA rapidly leading to recovery from the stalled condition, or at least a modulation of its extent. Once the leading edge shear layer is chopped by the wake, a vortex forms and propagates downstream, and with it, a pressure disturbance moves across the vane. As the vortex propagates downstream, the separation region at the leading edge begins to form and/or grow, a process which is interrupted by the arrival of the next blade wake.

Vane Unsteady Lift

To investigate the effect of mean loading on rotor blade wake generated unsteady lift, the vane surface unsteady pressures are measured over a range of mean flow AOA and spanwise locations. The unsteady pressure data are ensemble averaged and Fourier transformed into the frequency domain to obtain the rotor blade-pass harmonics. The vane surface unsteady and differential pressures are nondimensionalized by the freestream mean dynamic pressure,

$$p^*(x) = P_0(x) \Big/ \tfrac{1}{2}\rho_0 U^2 \qquad \Delta p^*(x) = \Delta p_0(x) \Big/ \tfrac{1}{2}\rho_0 U^2 \tag{3}$$

where $p(x)$ is the chordwise pressure distribution. The unsteady dimensionless lift is then calculated,

$$L = \int_{0.025}^{0.95} \Delta p^*(x^*)\, \mathrm{d}x^* \tag{4}$$

where $x^* = x/C$.

To normalize the unsteady pressure by the measured gust, the vane surface unsteady and differential pressures are nondimensionalized by the unsteady tangential measured velocity perturbation v_m^* at the vane leading edge at the given spanwise location and the midspan freestream density and flow velocity U. Therefore, the unsteady pressure coefficient is

$$C_p(x) = p^*(x) \Big/ \left(2v_m^+ \Big/ U\right) = p_0(x) \Big/ \rho_0 U v_m^* \tag{5}$$

$$C_{\Delta p}(x) = \Delta p^*(x) \Big/ \left(2v_m^+ \Big/ U\right) = \Delta p_0(x) \Big/ \rho_0 U v_m^* \tag{6}$$

where $\Delta p(x) = p(x)_{\text{lower}} - p(x)_{\text{upper}}$. The unsteady lift coefficient is then calculated from

$$C_L = \frac{L}{\left(2v_m^+ / U\right)} = \int_{0.025}^{0.95} C_{\Delta p}(x^*)\, \mathrm{d}x^* \tag{7}$$

Figures 12–14 present portraits of the unsteady lift as described by the lift coefficient as a function of instantaneous AOA. For comparison purposes, the steady (no rotor wake) and time-mean values of lift coefficient are also presented in Figs. 12–14 as a function of the mean AOA. In all cases, the unsteady coefficient of lift fluctuates

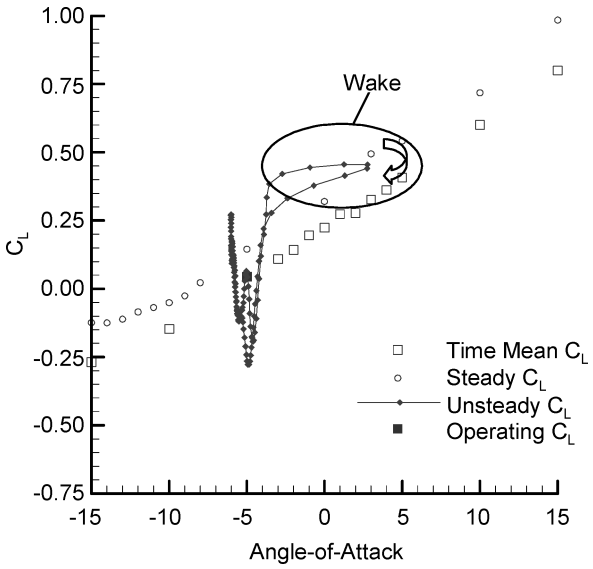

Fig. 12 Unsteady lift coefficient as a function of instantaneous AOA: −5 deg AOA (−17 deg stagger) and 50% span.

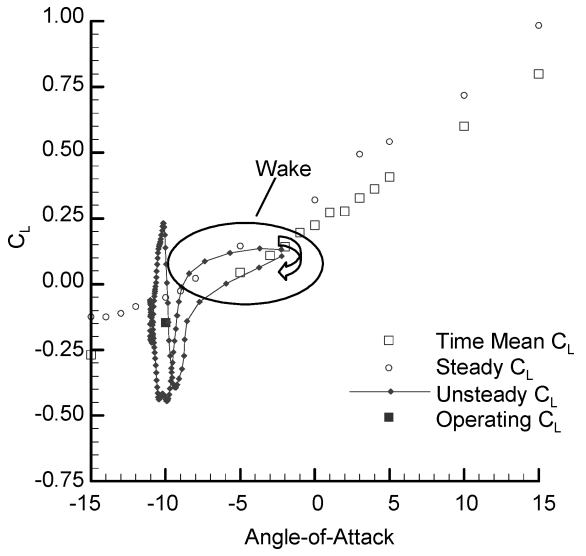

Fig. 13 Unsteady lift coefficient as a function of instantaneous AOA: −10 deg AOA (−22 deg stagger) and 50% span.

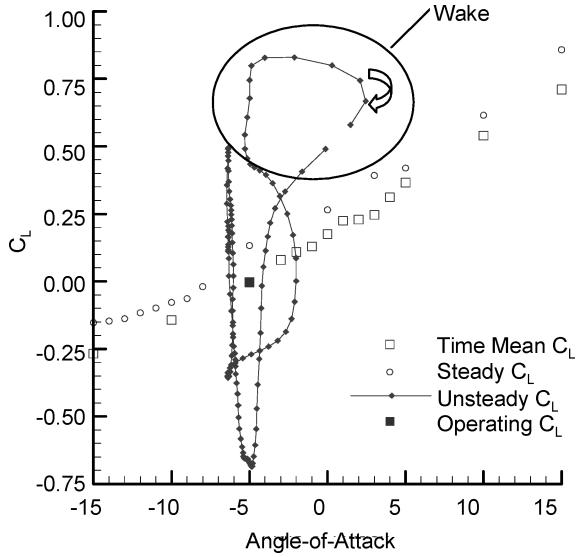

Fig. 14 Unsteady lift coefficient as a function of instantaneous AOA: −5 deg AOA (−17 deg stagger) and 90% span.

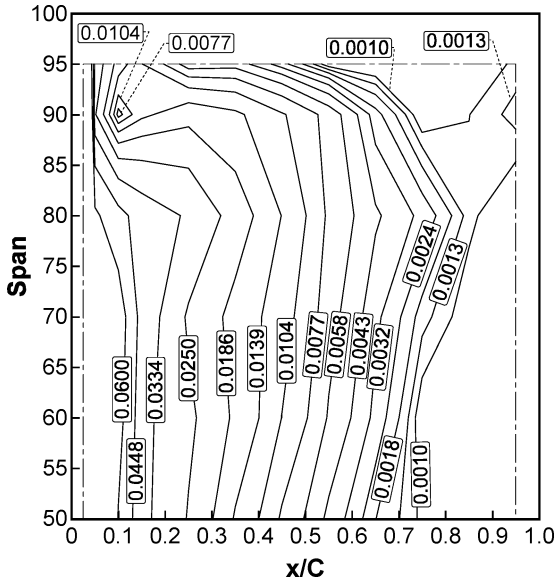

Fig. 15 First harmonic pressure magnitude as a function of span and chord, −5 deg AOA (−17 deg stagger).

widely throughout the blade-pass cycle. As the wake passes and the dynamic stall vortex begins to propagate downstream, the lift decreases sharply to the maximum negative value. This increase to the maximum lift as the dynamic stall vortex propagates downstream is how the turbomachinery dynamic stall is similar to the isolated airfoil dynamic stall, that is, the interaction of a strong vortex with the airfoil is similar, but the method of shedding this vortex is inherently different. This is most clearly seen in the unsteady coefficient of lift vs AOA in Fig. 12 for −5 deg mean AOA. As the wake hits the leading edge of the vane, the stall recovery occurs. Initially the airfoil recovers following the lift curve slope. As the vortex is shed, the lift recovers at a faster rate and decreases to the maximum negative point with subsequent fluctuations a result of the vortex propagation downstream.

A large negative lift is also achieved immediately following the wake at −10 deg mean AOA in Fig. 13. However, the maximum lift occurs much later in the cycle when the vortex has propagated near the trailing edge. The wake region is no longer the region of highest lift mainly due to the high negative loading on the vane and the persistent stall bubble at the leading edge.

Three-dimensional effects are also significant in turbomachinery and are increasingly important as newer designs at the back stages

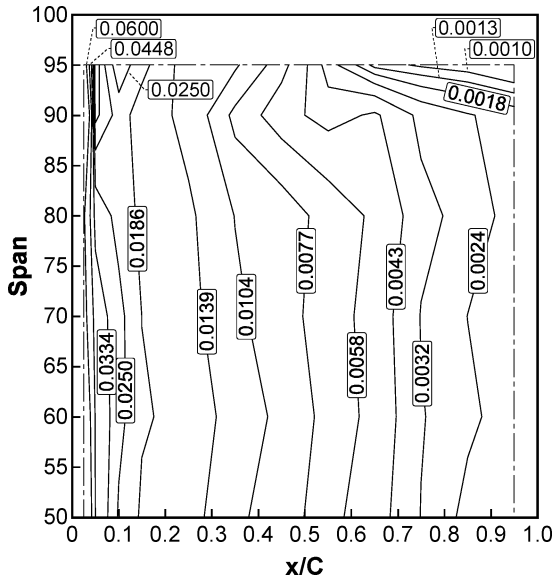

Fig. 16 First harmonic pressure magnitude as a function of span and chord, −10 deg AOA (−22 deg stagger).

of the compressors tend toward low aspect ratio blading. The three dimensionality of the forcing function was discussed earlier in this paper. Now the response is shown at 90% span at −5 deg mean AOA in Fig. 14. The unsteady fluctuation in lift is double that at midspan with little increase in magnitude of the forcing function from that at midspan. As at midspan, the wake hitting the vane causes the section lift to decrease to the maximum. The primary difference at 90% span is the effect of the dynamic stall vortex interacting with the endwall. The exceptionally high-lift fluctuations at 90% span may be explained by viewing the first harmonic pressure distributions.

The first harmonic pressure magnitude, $p^*(x)$, is shown in Figs. 15 and 16 for the pressure surface as a function of span and chord. Figure 15 shows that at −5 deg mean AOA, a clearly defined local minimum occurs at 90% span and 15% chord. At −10 deg mean AOA (Fig. 16), the local minimum in the first harmonic magnitude is seen from 90 to 95% span. In both cases, three-dimensional response is observed, with the variations of greatest extent for the −5 deg case.

Conclusions

This research was directed at understanding the three-dimensional effects and off-design conditions producing dynamic stall on the high-camber vane row due to the upstream high-camber rotor. These goals were reached by conducting experiments in a rotating annular cascade that is capable of reproducing the unsteady phenomena inherent in real turbomachinery cascades.

The three-dimensional unsteady flowfield behind a highly cambered rotor was characterized to describe the forcing function to the responding high-camber stator cascade. Data were taken at the vane leading edge with the vane row removed so only the forcing function of the rotor is measured, and vane potential effects are, therefore, not present in the forcing function data. The forcing function was found to be highly three dimensional especially near the tip region. Some of the three dimensionality in the forcing function at the tip was attributed to a rotor tip vortex.

The steady and unsteady surface pressures were measured on the vane with miniature pressure transducers mounted into the vane. The pressure data reinforces the portrait of the dynamic stall phenomena observed in part 1 of this paper (Ref. 7) namely, that the dynamic stall is driven by the wake passing the leading edge of the airfoil. This wake triggered dynamic stall is a result of the wake decreasing the magnitude of the AOA rapidly leading to recovery from the stalled condition, or at least a modulation of its extent. Once the leading-edge shear layer is chopped by the wake, a vortex forms and propagates downstream and with it a pressure disturbance

moves across the vane. As the vortex propagates downstream, the separation region at the leading edge begins to form and/or grow, a process which is interrupted by the arrival of the next blade wake.

The net effect of the dynamic stall condition is large fluctuations in unsteady lift as the process progresses. These variations were highly three dimensional, with the 90% span unsteady lift coefficient double that of midspan. As the wake hits the leading edge of the vane, stall recovery occurs. Initially, the slope of the recovery on the lift coefficient vs AOA matches that of the time mean lift characteristic curve. As the vortex is shed from the leading edge and begins to propagate downstream, the lift achieves a maximum negative value. Subsequent fluctuations in the lift are a result of the vortex interacting with the vane as it propagates downstream.

Acknowledgments

This research was sponsored by NASA John H. Glenn Research Center at Lewis Field and the Air Force Office of Scientific Research. This support is most gratefully acknowledged.

References

[1]Reynolds, W. C., and Carr, L. W., "Review of Unsteady, Driven, Separated Flows," AIAA Paper 85-0527, March 1985.

[2]Carr, L. W., and McCroskey, W. J., "A Review of Recent Advances in Computational and Experimental Analysis of Dynamic Stall," *Proceedings of the International Union of Theoretical and Applied Mechanics Symposium on Fluid Dynamics of High Angle of Attack*, Sept. 1992.

[3]Zaman, K. B. M. Q., Panda, J., and Rumsey, C. L., "Estimation of Unsteady Lift on a Pitching Airfoil from Wake Velocity Surveys," AIAA Paper 93-0437, Jan. 1993.

[4]Gendrich, C. P., Koochesfahani, M. M., and Visbal, M. R., "Initial Acceleration Effects on the Flow Field Development around Rapidly Pitching Airfoils," *Journal of Fluids Engineering*, Vol. 117, No. 1, 1995, pp. 45–49.

[5]Ehrlich, D. A., and Fleeter, S., "Incidence Effects on Chordwise Bending Cascade Unsteady Aerodynamics," *AIAA Journal*, Vol. 38, No. 2, 2000, pp. 284–291.

[6]Henderson, G. H., and Fleeter, S., "Vortical Gust Response of a Low-Solidity Vane Row Including Steady Loading and Dynamic Stall Effects," *Journal of Turbomachinery*, Vol. 119, No. 3, 1997, pp. 482–490.

[7]Key, N. L., Lawless, P. B., and Fleeter, S., "Rotor-Generated Vane Row Off-Design Unsteady Aerodynamics Including Dynamic Stall, Part 1," *Journal of Propulsion*, Vol. 20, No. 5, 2004, pp. 835–841.

[8]Henderson, G. H., "Forcing Function and Steady Loading Effects on Unsteady Aerodynamic Gust Response," Ph.D. Dissertation, Dept. of Mechanical Engineering, Purdue Univ., West Lafayette, IN, 1991.

[9]Chen, G. T., Greitzer, E. M., Tan, C. S., and Marble, F. E., "Similarity Analysis of Compressor Tip Clearance Flow Structure," *Journal of Turbomachinery*, Vol. 113, 1991, pp. 260–271.

[10]Visbal, M. R., "On Some Physical Aspects of Airfoil Dynamic Stall," Vol. 92, ASME Fluids Engineering Div., American Society of Mechanical Engineers, Fairfield, NJ, June 1990, pp. 127–147.